

# DCT-Based Iris Recognition

Donald M. Monro, *Member, IEEE*, Soumyadip Rakshit, *Student Member, IEEE*, and Dexin Zhang, *Student Member, IEEE*

**Abstract**—This paper presents a novel iris coding method based on differences of discrete cosine transform (DCT) coefficients of overlapped angular patches from normalized iris images. The feature extraction capabilities of the DCT are optimized on the two largest publicly available iris image data sets, 2,156 images of 308 eyes from the CASIA database and 2,955 images of 150 eyes from the Bath database. On this data, we achieve 100 percent Correct Recognition Rate (CRR) and perfect Receiver-Operating Characteristic (ROC) Curves with no registered false accepts or rejects. Individual feature bit and patch position parameters are optimized for matching through a product-of-sum approach to Hamming distance calculation. For verification, a variable threshold is applied to the distance metric and the False Acceptance Rate (FAR) and False Rejection Rate (FRR) are recorded. A new worst-case metric is proposed for predicting practical system performance in the absence of matching failures, and the worst case theoretical Equal Error Rate (EER) is predicted to be as low as  $2.59 \times 10^{-4}$  on the available data sets.

**Index Terms**—Biometrics, iris recognition, discrete cosine transform, image preprocessing, statistical analysis.

## 1 INTRODUCTION

PATTERN recognition methods can be classified into semantic and nonsemantic approaches. The use of the Karhunen-Loeve Transform (KLT) for object recognition [1] and, in particular, face recognition [2], are examples of nonsemantic techniques. The advantage of such methods arises from the automatic generation of suitable feature vectors by the KLT. Advanced feature extraction techniques find extensive use in the increasingly important domain of biometric identity authentication. As security becomes an issue of importance, biometrics [3], [4], [5] and iris recognition in particular are attracting great interest [6]. The human iris, a thin circular diaphragm lying between the cornea and the lens, has an intricate structure with many minute characteristics such as furrows, freckles, crypts, and coronas [7]. For every subject, these characteristics are unique as a result of the individual differences that arise in the development of anatomical structures during embryonic development. Apart from general textural appearance and color [8], the finely detailed structure of an iris is not genetically determined but develops by a random process. The iris patterns of the two eyes of an individual or those of identical twins are completely independent and uncorrelated [9]. Additionally, the iris is highly stable over a person's lifetime and lends itself to noninvasive identification because it is an externally visible internal organ.

Pioneering work on iris recognition was done by Daugman using Gabor wavelets [10], [11], [12]. That system has since been widely implemented and tested. Recently, other researchers including Wildes [13], Boles and Boashash [14], [15], Ma et al. [16], [17], and Monro and Zhang [18] have contributed new methods including ones based on the

application of PCA and ICA to iris images [19], [20]. Compared with other biometric technologies, such as fingerprint, face, hand-geometry, etc., iris recognition can easily be considered a reliable form of biometric technology. However, some critical problems still persist and significant work needs to be done before mass-scale deployment on national and international levels can be achieved [21]. Many issues, including system robustness, consistent performance under variability, speed of enrolment and recognition, and noncooperative identification remain to be addressed.

This paper contributes a realizable solution to some of these problems. Here, we investigate a novel method for iris matching using zero crossings of a one dimensional Discrete Cosine Transform (DCT) as a means of feature extraction for later classification. The DCT of a series of averaged overlapping angular patches are taken from normalized iris images and a small subset of coefficients is used to form subfeature vectors. Iris codes are generated as a sequence of many such subfeatures, and classification is carried out using a weighted Hamming distance metric. System parameters are optimized to give lowest equal error rates (EER) on two data sets.

The paper is subdivided into the following sections: Section 2 summarizes the use of the DCT. Section 3 describes the data collection carried out at the University of Bath in working toward a large, varied, and high-quality publicly available iris image database. The following section gives an overview of the process of iris normalization resulting in a fixed rectangular enhanced normalized image. Section 5 details the proposed iris coding method along with parameter optimizations and classifier specifications. Evaluations with statistical analyses follow in Section 6. Finally, in Section 7, we draw conclusions and give suggestions for future work.

## 2 THE DISCRETE COSINE TRANSFORM

The DCT is a real valued transform, which calculates a truncated Chebyshev series possessing well-known minimax properties and can be implemented using the Discrete Fourier Transform (DFT) [22]. There are several variants

• The authors are with the Department of Electronic and Electrical Engineering, University of Bath, Claverton Down, Bath, BA2 7AY, UK. E-mail: {d.m.monro, s.rakshit}@bath.ac.uk.

Manuscript received 3 Feb. 2006; revised 14 July 2006; accepted 26 Sept. 2006; published online 18 Jan. 2007.

Recommended for acceptance by S. Prabhakar, J. Kittler, D. Maltoni, L. O'Gorman, and T. Tan.

For information on obtaining reprints of this article, please send e-mail to: tpami@computer.org and reference IEEECS Log Number TPAMISI-0118-0206. Digital Object Identifier no. 10.1109/TPAMI.2007.1002.

TABLE 1  
Breakdown of Bath Database (200 Subjects)

Age	%	Ethnicity	%	Sex	%
16-25	57.2	White	67.2	Female	48.3
26-35	22.5	Black	8.0		
36-45	8.7	South Asian	3.6		
46-55	5.1	Oriental	15.3	Male	51.7
56-65	6.5	Others	5.9		

but the one most commonly used operates on a real sequence  $x_n$  of length  $N$  to produce coefficients  $C_k$ , following Ahmed et al. [23]:

$$C_k = \frac{2}{N} w(k) \sum_{n=0}^{N-1} x_n \cos\left(\frac{2n+1}{2N} \pi k\right), \quad 0 \leq k \leq N-1$$

and

$$x_n = \sum_{k=0}^{N-1} w(k) C_k \cos\left(\frac{2n+1}{2N} \pi k\right), \quad 0 \leq n \leq N-1,$$

where

$$w(k) = \sqrt{2}, \quad k=0 \text{ and } w(k) = 1, \quad 1 \leq k \leq N-1.$$

Due to its strong energy compaction property, the DCT is widely used for data compression. In addition, the feature extraction capabilities of the DCT coupled with well-known fast computation techniques [24], [25], [26] have made it a candidate for pattern recognition problems such as the one addressed here. In particular, the DCT has been shown to produce good results on face recognition [27], [28], where it has been used as a less computationally intensive replacement for the Karhunen-Loeve transform (KLT), which is an optimal technique according to the least squares metric for projecting a large amount of data onto a small dimensional subspace [1], [29]. The KLT decomposes an image into principal components ordered on the basis of spatial correlation and is statistically optimal in the sense that it minimizes the mean square error between a truncated representation and the actual data [22]. The DCT, with its variance distribution closely resembling that of the KLT, has been shown to approach its optimality with much lower computational complexity [30]. Additionally, its variance distribution decreases more rapidly compared to other deterministic transforms [22]. Although no transform can be said to be optimal for recognition, these well-known properties motivated us to investigate the DCT for effective nonsemantic feature extraction from human iris images.

### 3 DATA COLLECTION

A major hindrance to research in the field of iris recognition has been a shortage of publicly available images. With other biometrics such as face and fingerprints, there is access to thousands of images from various sources, but, until recently, the only readily available source of iris images has been the CASIA database [31]. Although this data set has proven to be invaluable, its lack of variety may have led to the design of somewhat biased systems. Our studies suggest that any

algorithm optimized for an image-set consisting primarily of one type of iris, Asian, in this case, will be inherently biased toward a particular pattern and may not be effective when applied to a more diverse database. Recently, other iris image data sets have been assembled [32], [33], [34], [35], [36]. As a contribution to this process, we are gathering high quality iris images from students and staff of the University of Bath comprising subjects from a variety of backgrounds [37]. At the time of writing, more than 800 classes have been collected, of which a subset of 150 were available for the experiments described here. The age, ethnicity, and gender breakdown of a superset is tabulated in Table 1 to give an indication of the diversity of those members of a similar population who were willing to give this information.

It is known that images of the human iris obtained with Near-Infrared (NIR) lighting are necessary to reveal complex textures for darkly pigmented irises, while lighter irises can be imaged either in the infrared or visible spectrum [12]. In collecting the Bath database, eyes are imaged using an NIR sensitive high-resolution ( $1,280 \times 1,024$ ) machine-vision camera with infrared lighting whose spectrum peaks around 820 nm. Daylight cut-off filters are used to eliminate reflections due to ambient visible light and care is taken to focus on the iris rather than on any other part of the eye such as eyelids or eyelashes.

With the subject sitting and positioned against chin and forehead rests, the camera is manually positioned. A focal length of 35 mm, with the lens 20 cm from the eye, ensures that a large proportion of the image is that of the iris. The incoherent NIR light source is an array of LEDs close to the camera lens so that its reflections are within the boundary of the pupil with the subject looking into the lens. To avoid thermal injury, the power of infrared radiation in the range of 780 nm to 3  $\mu\text{m}$  should be limited to less than 10 mW/cm<sup>2</sup> according to US recommendations [38], [39]. A more stringent regulation for lasers (coherent light), widely followed in Europe, suggests a more conservative 0.77mW/cm<sup>2</sup> [40]. Measurements on our apparatus indicate that the power of the incoherent infrared radiation reaching the eye is less than 0.5mW/cm<sup>2</sup>. Due to the presence of ambient visible lighting, the pupil is partly constricted, thereby providing an additional safety mechanism.

With the camera manually lined up and focused, a video sequence of several seconds duration is collected. Suitable images from the video sequence are selected in two stages. First, to evaluate focus and motion blur, the area of the specular reflection within the pupil is measured and images with light-areas greater than an experimentally set cut-off are removed [41]. Specular reflection detection is carried out by searching for the largest positive change over a 5-pixel

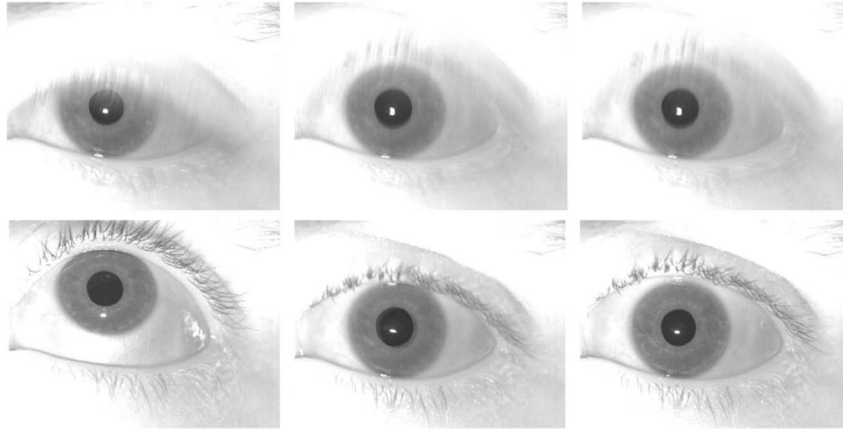


Fig. 1. Images taken from a video-sequence of an eye illustrating the variations in the size of the reflected light source.

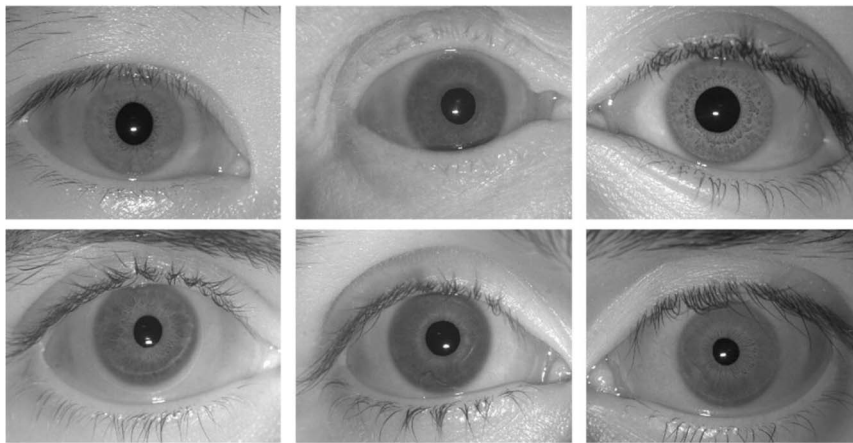


Fig. 2. Sample eye images from the Bath Database.

neighborhood for all rows with spurious results omitted by light shape analysis. As may be observed from the image sequence in Fig. 1, the light-area increases with eye-movement, eyelid occlusion, and focus-blur. A lack of light within the pupil is an indication that the eye is not properly centered.

In the second stage, the remaining images are normalized and tested for sharpness using a kurtosis measure of their 2D Fourier spectrum. Since the high spatial frequency components of a sharper image are larger than those of a blurred one, a 2D spatial Fourier frequency magnitude distribution for a sharp image has a wider envelope. For a given univariate random variable, the kurtosis is defined as the ratio of the fourth and squared second central moments [42]. Treating the normalized spatial spectrum as a probability density function, a sharper iris thus corresponds to a spectrum with a flatter shape and smaller kurtosis. The images are sorted according to their kurtosis value in ascending order and 20 are accepted from the highest ranked images for each eye by manual inspection. Sample images from the Bath database are shown in Fig. 2.

#### 4 IMAGE PREPROCESSING

For coding, irises are extracted from the eye images and normalized to a standard format for feature extraction in order to remove variability introduced by pupil dilation, camera-to-eye distance, head tilt, and torsional eye rotation

within its socket [10], [11]. Moreover, images acquired by different cameras under different environmental conditions have different resolution and illumination distributions [13], [17]. All these factors need to be taken into consideration and compensated for in order to generate a final normalized version compliant with the feature extraction input format. Iris images already normalized to a resolution of  $512 \times 80$  pixels for 308 classes were obtained from CASIA, and the 150 classes from the Bath database were preprocessed in-house. A full description of the preprocessing method is beyond the scope of this paper; below is a summary as illustrated by Fig. 3.

##### 4.1 Localization

Location of the pupil and outer iris boundaries starts with the removal of the bright spot in the pupil caused by the reflection of the infrared light source. This reduces the influence of high gray-level values on the gray-scale distribution. Then, the image is scanned to isolate a region containing the pupil and iris. This is done by a heuristic method based on the assumption that the majority of image rows and columns passing through the pupil will have larger gray-level variance than those not passing through the pupil. It is assumed that the pupil is circular and, because the pupil boundary is a distinct edge feature, a Hough transform is used to find the center and radius of the pupil. To locate the outer boundary of the iris (limbus), a

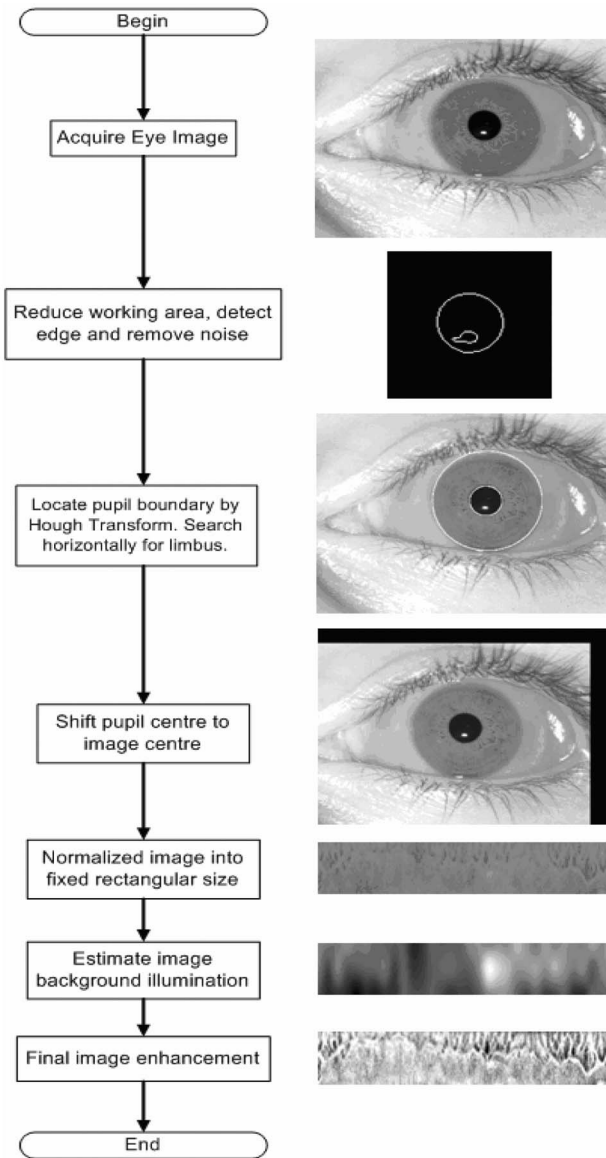


Fig. 3. Illustrating the various steps involved in the generation of a fixed rectangular enhanced normalized iris image.

horizontal line through the pupil center is scanned for the jumps in gray level on either side of the pupil. The limbus is normally circular but its center does not necessarily coincide with that of the pupil.

## 4.2 Normalization and Enhancement

Due to the dilation and constriction of the human pupil, the radial size of the iris varies under different illumination conditions and in response to physiological factors. The resulting deformation of the iris texture can be approximated as a linear deformation [43], [44]. Since we know the iris boundaries, we can map a rectangular image array back to an angular and radial position in the iris. This position will not, in general, map exactly onto a pixel in the source image, so the normalized gray value is obtained by bilinear interpolation from its four nearest neighbors. Finally, the gray levels are adjusted by removing the peak illumination caused by light sources reflecting from the eye, estimating and subtracting the slowly varying background illumination, and equalizing the gray-level histogram of the iris image. The final normal-

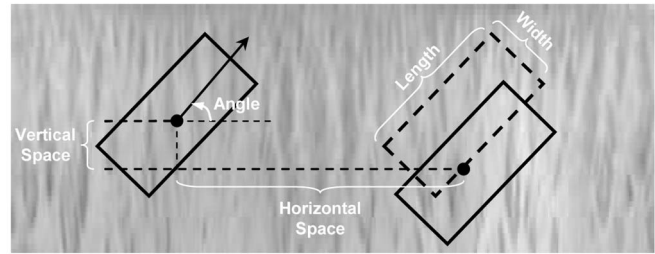


Fig. 4. Overlapping angular Patches with their various parameters.

ized image is of resolution  $512 \times 80$ , from which we code only the 48 rows nearest the pupil to mitigate the effect of eyelids.

## 5 PROPOSED IRIS CODING METHOD

The human iris, being highly specific to an individual, needs to be coded to exploit the local textural variations while keeping complexity to a minimum. The primary objective behind any good iris coding method is to obtain good interclass separation in minimum time. As explained earlier, the DCT, being an approximation to the KLT, is a good candidate for feature extraction and is thus used here as a means of representing the intricate and detailed variations in the human iris texture. In our earlier work, based on Fourier-domain methods [18], good results were obtained. Here, we discuss the use of the new method in generating an iris-code with various parameter optimizations and weightings to give further improved performance.

### 5.1 Feature Extraction

As in our Fourier-based iris coding work [18], we start from a general paradigm whereby the feature vectors will be derived from the zero crossings of the differences between 1D DCT coefficients calculated in rectangular image patches, as illustrated by Fig. 4. Averaging across the width of these patches with appropriate windowing helps to smooth the data and mitigate the effects of noise and other image artifacts. This then enables us to use a 1D DCT to code each patch along its length, giving low-computational cost. The selection of the values for the various parameters was done by extensive experimentation over the CASIA and Bath databases to obtain the best predicted Equal Error Rate (EER). The two data sets were used in their entirety to optimize the parameters of the method.

Experimentally, overlapping patches gave the best EER in combination with the other parameters. It was also found that horizontally aligned patches worked best, and a rotation of 45 degrees was better than 0 degrees or 90 degrees. This distinctive feature of our code introduces a blend of radial and circumferential texture allowing variations in either or both directions to contribute to the iris code.

To form image patches, we select bands of pixels along 45 degree lines through the image. A practical way of doing this is to slew each successive row of the image by one pixel compared to its predecessor. Patches are then selected in 11 overlapping horizontal bands as in Fig. 5. Each patch has eight pixels vertically (overlapping by four) and 12 horizontally (overlapping six). In the horizontal direction, a weighted average under a  $1/4$  Hanning window is formed. In effect, the resolution in the horizontal (iris circumferential) direction is reduced by this step. Averaging across the width

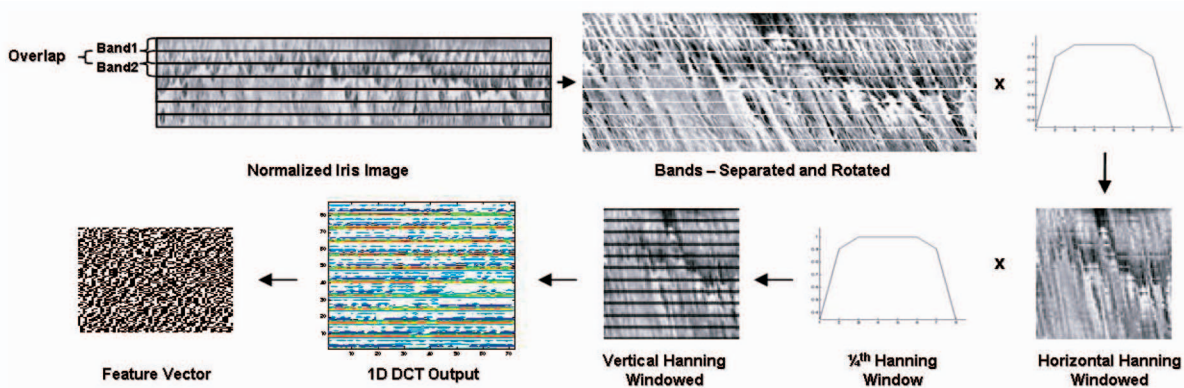


Fig. 5. Illustrating the various steps in forming feature vectors from normalized iris images.

of the patch helps to reduce the degrading effects of noise and the use of broad patches makes for easier iris registration. In the vertical direction (45 degrees from the iris radial), eight pixels from each patch form a 1D patch vector, which is then windowed using a similar Hanning window prior to application of the DCT in order to reduce spectral leakage during the transform. The differences between the DCT coefficients of adjacent patch vectors are then calculated and a binary code is generated from their zero crossings. These 8-bit code fragments (codelets) are the basis of our matching process, but are further trimmed as described at *C* below.

## 5.2 Matching

For comparing two iris codes, a nearest-neighbor approach is taken, where the distance between two feature vectors is measured using the product-of-sum (POS) of individual subfeature Hamming distances (HD). This can be defined as follows:

$$HD = \left( \prod_{i=1}^M \frac{\sum_{j=1}^N (SubFeature_{1ij} \oplus SubFeature_{2ij})}{N} \right)^{1/M}$$

Here, we consider the iris code as a rectangular block of size  $M \times N$ ,  $M$  being the number of bits per subfeature and  $N$  the total number of subfeatures in a feature vector. Corresponding subfeature bits are XORed and the resultant  $N$ -length vector is summed and normalized by dividing by  $N$ . This is done for all  $M$  subfeature bits and the geometric mean of these  $M$  sums give the normalized HD lying in the range of 0 to 1. For a perfect match, where every bit from Feature 1 matches with every corresponding bit of Feature 2, all  $M$  sums are 0 and so is the HD, while, for a total opposite, where every bit from the first Feature is reversed in the second,  $MN/Ns$  are obtained with a final HD of 1. Since a total bit reversal is highly unlikely, it is expected that a random pattern difference should produce an HD of around 0.5.

While our previous approach [18] based the HD calculation on a weighted sum of EXOR-ed bits, the new POS method provides for better separation by skewing the matching distribution toward 0 and the nonmatching one toward 0.5. A side-effect of taking the geometric mean is that an identical match between any two corresponding sets of  $N$  subfeature bits will give an overall HD of 0 and, thus, a perfect match. Although this might seem radical, it is highly unlikely that all  $N$  bits, 713 in this case, will match identically for any two iris

templates. Even if such a situation were to occur, it is very likely that both templates originated from the same class.

Rotation invariance is achieved by storing six additional iris codes for three rotations on either side by horizontal (iris circumferential) shifts of 4, 8, and 12 pixels each way in the normalized images. During verification, the test iris code is compared against all seven stored ones and the minimum distance is chosen for each of the three separately enrolled images. These three minima are then averaged to give the matching HD.

## 5.3 Optimized DCT Coefficients

To reduce the feature vector length, the most discriminating binarized DCT coefficients are extracted and the remaining ones are discarded. Extensive experiments were undertaken to determine the most effective combinations of bits to form subfeature vectors from the codelets. To do this, the entire set of test data was coded for every combination of codelet bits ranging from selecting any one bit to using all bits. The bit combination producing the best separation between the matching and nonmatching Hamming distances was chosen as the final subfeature. This is illustrated by Fig. 6, in which one test iris is matched against the entire data set and the HD sum for each codelet bit is plotted separately.

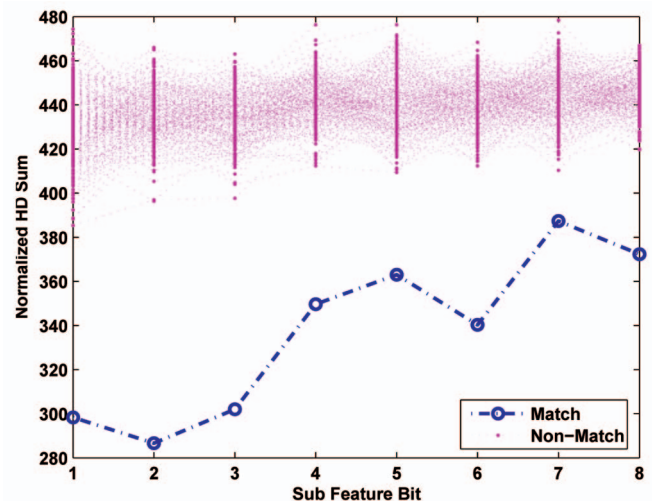


Fig. 6. Illustrating the discriminating bits in an 8-bit codelet for one test image. Greater separation between matching and nonmatching plots indicates better discrimination.

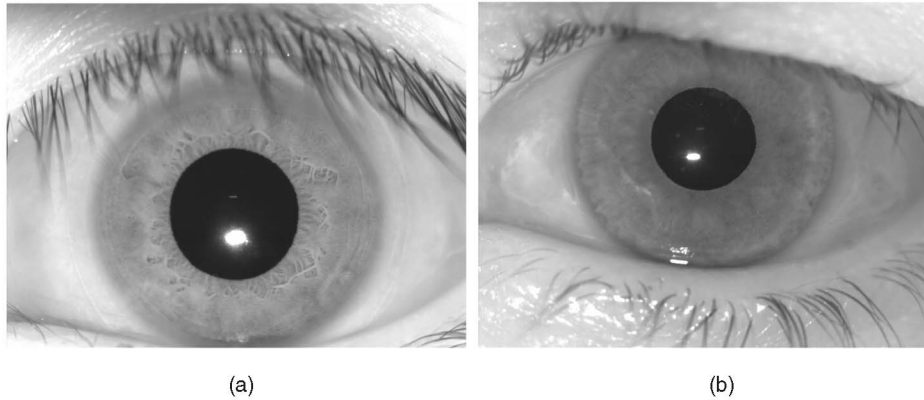


Fig. 7. Different iris textures in (a) Asian (brown) iris and (b) Western (Blue/Green) eyes.

The matching curve was found to be well separated from the nonmatching one for the first three bits with decreasing separation thereafter for higher order bits corresponding to high frequency zero crossings as shown in Fig. 6.

The final feature vector selected for our method is formed using 3-bit subfeatures consisting of bits 1-3. With 781 such subfeatures in total, the feature length is 2,343 bits. Since the first and second bits are individually very discriminating, the subfeature length could be reduced further by using only the first bit or the first two bits with an expected increased in speed of operation at reduced accuracy.

#### 5.4 Positional Weighting

Visual inspection of iris images from the Bath Database indicate that Asian (generally, brown) irises have more texture (contraction furrows) toward the pupil with little texture on the periphery, while western (blue/green) irises have thin yet uniform sinuously radiating fibers throughout, as illustrated in Fig. 7. Much of the published work on iris recognition is based on the CASIA data set, which is biased toward Asian eyes. In particular, our previous work [18] was based on CASIA and weighed the iris patches nearer to the pupil more heavily than the ones further away from it. Using the new Bath Database, it was observed that better overall performance can be achieved by removing any such weighting so that the method is not biased toward any particular iris texture pattern.

## 6 RESULTS

To evaluate our method, we first applied it to the widely used CASIA database consisting of 308 classes (eyes) and then to the more varied Bath database which consisted of 150 classes at the time of the experiments. For both data sets, three arbitrary images were chosen in each case from each class to be enrolled in the database for matching, leaving the rest for testing. Both Identification and Verification tests were carried out. For Identification, a test image was coded and compared against the whole database of stored features. The comparison resulting in the lowest average Hamming distance across the three enrolled images for each class was chosen as the matching iris. One hundred percent Correct Recognition Rates were obtained on both the CASIA and Bath data sets. For Verification, Receiver Operating Characteristic (ROC) curves were generated by varying a match-cut-off threshold from 0 to 1 and plotting

the False Rejection Rate (FRR) as a function of the False Acceptance Rate (FAR). At a given threshold, the FAR and FRR indicate the probability of accepting an imposter and rejecting a genuine person, respectively, [45].

Fig. 8 illustrates the ROC curves on the CASIA database for the three algorithms compared, namely, Daugman, Tan, and the one proposed. The Daugman and Tan algorithms implemented in MATLAB were obtained from Li Ma of CASIA, as used in [16], for which he tuned the parameters of the Daugman Gabor filters for optimum EER performance on the CASIA database.

All comparisons were carried out at the feature extraction level on the same set of prenormalized images in order to achieve a fair comparison. In these results, a single false rejection causes a step jump of 0.08, while three false rejects cause a rise of 0.24. These small numbers of failures are not sufficient for drawing statistically significant comparisons but are shown in keeping with the general practice of showing ROC curves for comparing algorithms. Similar curves are obtained on the Bath database. Due to the lack of false accepts when there are false rejects and vice versa, our characteristic is entirely on the  $FRR = 0$  axis.

Performance is better illustrated by showing the Hamming Distances for all matches as shown in Fig. 9. The three plots in each case represent the matching, nearest

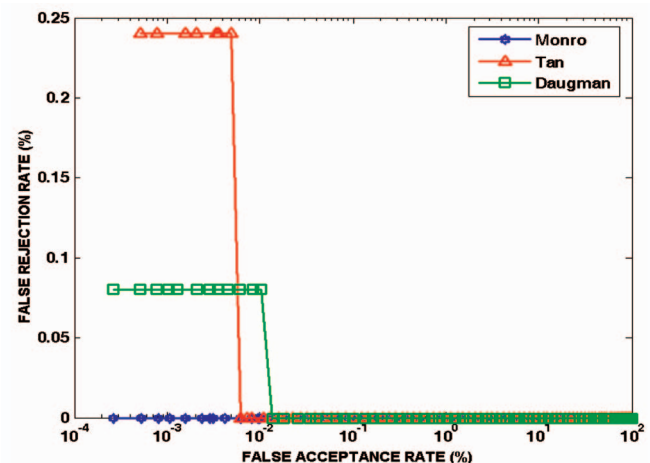
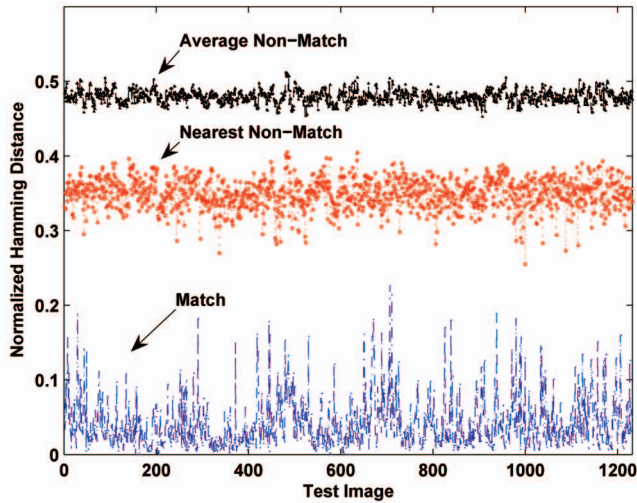
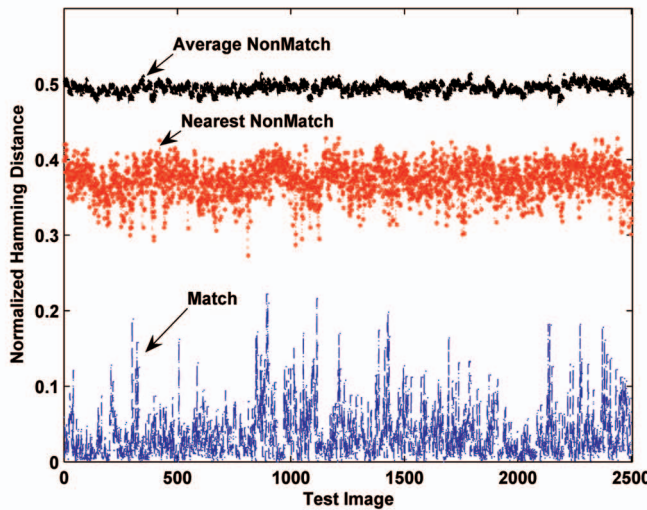


Fig. 8. Receiver Operating Characteristics for the methods of Daugman, Tan, and the proposed DCT algorithm. Both competitive algorithms were implemented in-house based on published literature.



(a)

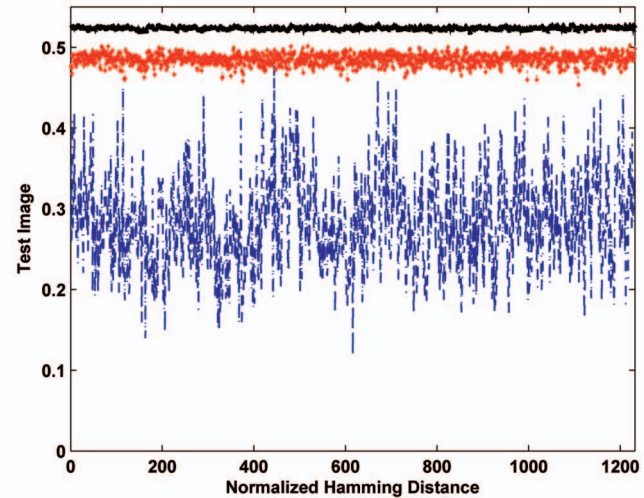


(b)

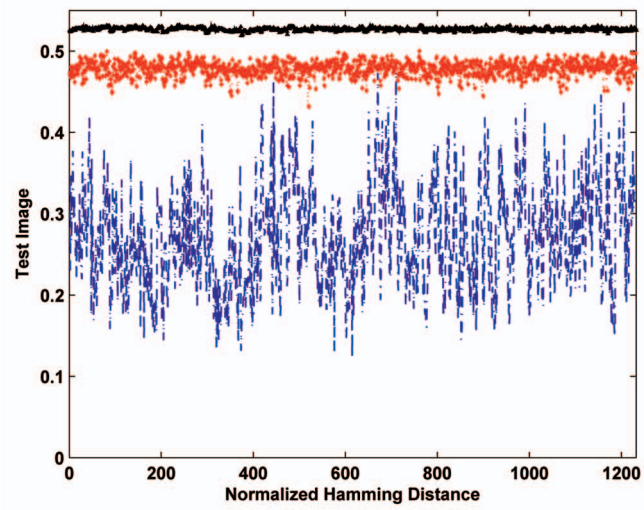
Fig. 9. Hamming distances for all classes in (a) CASIA and (b) Bath databases.

nonmatching, and average nonmatching normalized Hamming distances for all test images. Similar Plots for the Daugman and Tan algorithms are shown in Fig. 10. It is evident from these plots that the matching and nearest nonmatching data are not as well separated by the Daugman and Tan algorithms in the implementations we used as they are by the proposed DCT code.

It is common for the separation of the average nonmatch from the match to be used as a figure of merit for biometrics [10], [11]. However, the distance between the match and the nearest nonmatch is a more stringent test. This shows the lowest HD from a nonmatching test class when compared with the original enrolled one. This is a more realistic comparison because real systems fail when the HD of the nearest nonmatch falls below the HD of the correct match. Since there is a distinct band of white space between the two plots for both the CASIA and Bath results, it means that, for a range of match-thresholds, there will be no false accepts or rejects as neither plot will cross over to the other side for any test image.



(a)



(b)

Fig. 10. Hamming distances for all classes in the CASIA database for the (a) Daugman and (b) Tan algorithms.

An important figure of merit for the biometric system is the Equal Error Rate (EER), which is the FAR and FRR when they are equal. As in Fig. 8, the actual EER cannot accurately be estimated when there are no failures or only a few failures. In the absence of thousands or millions of cases for testing, the EER must be predicted by statistical modeling. In Fig. 11, we show two probability distributions for the Hamming distance, one for matching and the other for nearest nonmatching irises. With each distribution normalized for unit area, the area under the matching distribution above a chosen HD threshold ( $\tau$ ) is the FRR, while the area under the nonmatching distribution below the threshold is the FAR. The EER is the area such that the integral from  $-\infty$  to  $\tau$  of the nonmatching distribution is equal to the integral from  $\tau$  to  $\infty$  for the matching distribution. When the nonmatching distribution is the nearest nonmatch, the EER is a more stringent metric than if the average nonmatch is used, and we call this the worst-case EER.

Experimental observations show that for, our system, the Gamma distribution best describes the distribution of

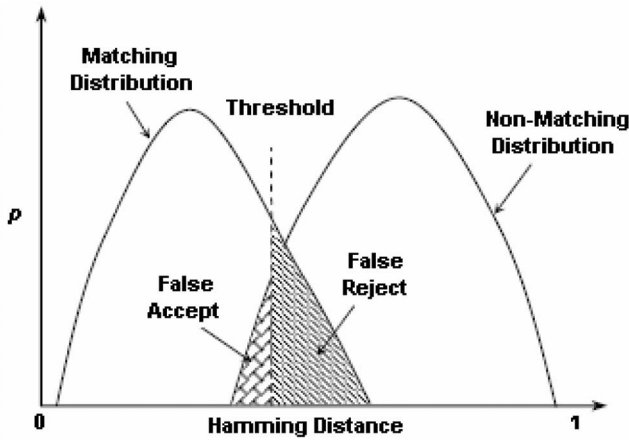


Fig. 11. False Accept and Reject distributions.

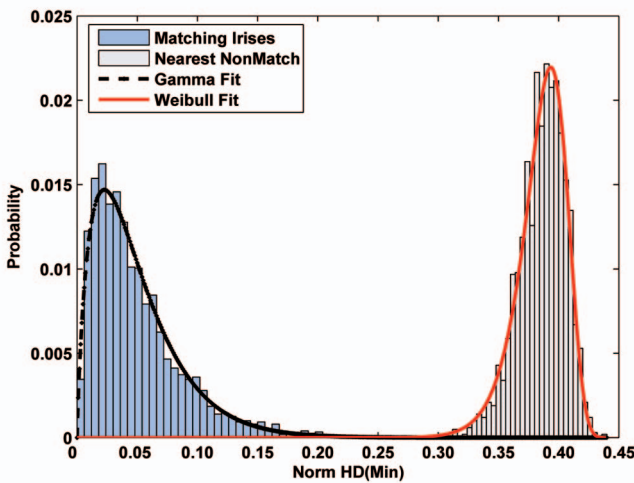


Fig. 12. Probability distribution curves for matching and nearest nonmatching Hamming distances. Gamma (1.84, 26.87) and Weibull (394.85, 23.58) probability density functions used to model the two data are shown as overlapping plots.

matching Hamming distances in a least square error sense, while a Weibull distribution is the best fit for the nearest nonmatch. The best fit curves for the Bath database are shown in Fig. 12; those for CASIA are very similar. The EERs obtained for the Bath and CASIA data sets are  $2.59 \times 10^{-4}$  and  $5.55 \times 10^{-4}$ , respectively. For comparison, on the CASIA data set, we estimate the EER as  $8.9 \times 10^{-3}$  for the Tan method and  $4.9 \times 10^{-3}$  for the Daugman algorithm. It must be noted here that these estimates are based on the more stringent and practically relevant basis of the nearest nonmatch.

In Table 2, we compare the speed of our MATLAB implementations of the three algorithms studied here. The Feature extraction times are found by running the code on the entire CASIA data set and dividing by the total number of images (2,156). For matching, all possible matches of 308 classes against 1,232 test images are made and the total time is divided by 379,456 ( $308 \times 1,232$ ). In all cases, we obtained mean values and standard deviations were not collected. We observe that the total time taken by feature extraction and matching is 61 ms as against 193 ms taken by the Tan method and 453 ms taken by Daugman’s algorithm on the same standard normalized CASIA test case using our implementations. The main speed gain occurs in the feature

TABLE 2  
Speed Comparison between Competing Methods

Method	Feature Extraction (ms)	Matching (ms)	Total (ms)
Daugman	422	31	453
Tan	125	68	193
Monro	30	31	61

extraction stage, where the simplicity of application of the 1D DCT helps speed up the entire process compared to the more computationally intensive procedures adopted by the other methods. The matching speeds are relatively similar due to the Hamming distance being adopted by all as the classification metric, depending only on the feature vector lengths, which, again, is equal or smaller by our method. It should be noted that all figures are based on MATLAB implementations and are to be interpreted on a relative scale only; implementations in real systems are likely to be many times faster.

## 7 CONCLUSIONS

In this paper, we have described an approach to human iris recognition based on the 1D Discrete Cosine Transform (DCT), which supersedes our earlier work in this field [18]. The work was motivated by the near-optimal decorrelating properties of the DCT compared to the Karhunen-Loeve transform, and the results achieved indicate the good performance of the approach in which there are no False Accepts/Rejects on the CASIA and Bath data sets used. The method as implemented also has low complexity, making it superior to the other methods evaluated in terms of both speed and accuracy.

We have demonstrated the use of novel patch encoding methods in capturing iris texture information, proposed the worst-case (nearest nonmatch) EER as a new practical metric for evaluating systems, and investigated better classifier designs for wider interclass separability. Statistical analysis has also been carried out to find the best models for matching and nonmatching probability distributions in order to predict worst-case equal error rates where no failures occur.

It is difficult to extract statistically significant performance estimates from data sets in which the failure rates are low. We can infer from Figs. 9 and 10 that the proposed method achieves a better separation of the matching and nearest nonmatching Hamming distances, as is also indicated by our estimates of the EER. Unfortunately, such very large data sets as may exist (tens of thousands or even millions of classes) are not available for security and/or proprietary reasons. Our use of a more stringent metric for comparing matching and nonmatching distributions is helpful in obtaining useful results from small data sets. This is also the reason why we did not partition the available data into training and test sets. Despite this, the numbers of failures are so low that it is not possible to make statistically significant claims about the relative performance of the methods tested. Because of the diversity of iris image sources and the limited size of public data sets, it is not yet possible to extrapolate the results to large

populations. Performance prediction will become more accurate as larger data sets become available.

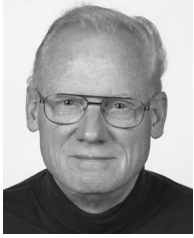
There remain many interesting problems in preprocessing human iris images which will further enhance the performance of this and other iris matching techniques. For implementation in real systems, the effects of nonideal image capture conditions await evaluation, either by simulation or in the field.

## ACKNOWLEDGMENTS

The authors are grateful to Professor Tieniu Tan of the Chinese Academy of Sciences Institute of Automation (CASIA) for use of the CASIA Iris Image Database on which some results are based and to Dr. Li Ma of CASIA for his implementations in MATLAB of the Tan and Daugman algorithms. This work was sponsored by Smart Sensors Limited, Portishead, Bristol BS20 7BA, United Kingdom.

## REFERENCES

- [1] M. Uenohara and T. Kanade, "Use of Fourier and Karhunen-Loeve Decomposition for Fast Pattern Matching with a Large Set of Templates," *IEEE Trans. Pattern Analysis and Machine Intelligence*, vol. 19, pp. 891-898, 1997.
- [2] M. Turk and A. Pentland, "Eigenspaces for Recognition," *J. Cognitive Neuroscience*, vol. 3, no. 1, pp. 71-86, 1991.
- [3] A.K. Jain, S. Pankanti, S. Prabhakar, L. Hong, A. Ross, and J.L. Wayman, "Biometrics: A Grand Challenge," *Proc. 17th Int'l Conf. Pattern Recognition*, vol. 2, pp. 935-942, 2004.
- [4] A.K. Jain, A. Ross, and S. Prabhakar, "An Introduction to Biometric Recognition," *IEEE Trans. Circuits and Systems for Video Technology*, vol. 14, pp. 4-20, 2004.
- [5] A. Ross and A.K. Jain, "Multimodal Biometrics: An Overview," *Proc. 12th European Signal Processing Conf.*, pp. 1221-1224, 2004.
- [6] *UK Passport Service Biometrics Enrollment Trial*, Atos Origin, May 2005.
- [7] F.H. Adler, *Physiology of the Eye*. Mosby, 1965.
- [8] P. Kronfeld, *Gross Anatomy and Embryology of the Eye*. Academic Press, 1962.
- [9] J. Daugman and C. Downing, "Epigenetic Randomness, Complexity, and Singularity of Human Iris Patterns," *Proc. Royal Soc. (London) B: Biological Sciences*, vol. 268, pp. 1737-1740, 2001.
- [10] J. Daugman, "High Confidence Visual Recognition of Persons by a Test of Statistical Independence," *IEEE Trans. Pattern Analysis and Machine Intelligence*, vol. 15, pp. 1148-1161, 1993.
- [11] J. Daugman, "The Importance of Being Random: Statistical Principles of Iris Recognition," *Pattern Recognition*, vol. 36, pp. 279-291, 2003.
- [12] J. Daugman, "Statistical Richness of Visual Phase Information: Update on Recognizing Persons by Iris Patterns," *Int'l J. Computer Vision*, vol. 45, pp. 25-38, 2001.
- [13] R.P. Wildes, "Iris Recognition: An Emerging Biometric Technology," *Proc. IEEE*, vol. 85, pp. 1348-1363, 1997.
- [14] W.W. Boles and B. Boashash, "A Human Identification Technique Using Images of the Iris and Wavelet Transform," *IEEE Trans. Signal Processing*, vol. 46, pp. 1185-1188, 1998.
- [15] W.W. Boles, "A Security System Based on Human Iris Identification Using Wavelet Transform," *Proc. First Int'l Conf. Knowledge-Based Intelligent Electronic Systems*, vol. 2, pp. 533-541, 1997.
- [16] L. Ma, T. Tan, Y. Wang, and D. Zhang, "Personal Identification Based on Iris Texture Analysis," *IEEE Trans. Pattern Analysis and Machine Intelligence*, vol. 25, pp. 1519-1533, 2003.
- [17] L. Ma, T. Tan, Y. Wang, and D. Zhang, "Efficient Iris Recognition by Characterizing Key Local Variations," *IEEE Trans. Image Processing*, vol. 13, pp. 739-750, 2004.
- [18] D.M. Monro and D. Zhang, "An Effective Human Iris Code with Low Complexity," *Proc. IEEE Int'l Conf. Image Processing*, vol. 3, no. 3, pp. 277-280, 2005.
- [19] J. Cui, Y. Wang, J. Huang, T. Tan, and Z. Sun, "An Iris Image Synthesis Method Based on PCA and Super-Resolution," *Proc. 17th Int'l Conf. Pattern Recognition*, vol. 4, pp. 471-474, 2004.
- [20] Y. Huang, S. Luo, and E. Chen, "An Efficient Iris Recognition System," *Proc. Int'l Conf. Machine Learning and Cybernetics*, vol. 1, pp. 450-454, 2002.
- [21] "Independent Testing of Iris Recognition Technology Final Report," Int'l Biometric Group, May 2005.
- [22] K.R. Rao and P. Yip, *Discrete Cosine Transform: Algorithms, Advantages, Applications*. Academic, 1990.
- [23] N. Ahmed, T. Natarajan, and K. Rao, "Discrete Cosine Transform," *IEEE Trans. Computers*, vol. 23, pp. 90-93, 1974.
- [24] A.C. Hung and T.H.-Y. Meng, "A Comparison of Fast Inverse Discrete Cosine Transform Algorithms," *Multimedia Systems*, vol. 2, pp. 204-217, 1994.
- [25] M. Vetterli, "Fast 2-D Discrete Cosine Transform," *Proc. IEEE Int'l Conf. Acoustics, Speech, and Signal Processing*, pp. 1538-1541, 1985.
- [26] Z. Yonghong, C. Lizhi, B. Guoan, and A.C. Kot, "Integer DCTs and Fast Algorithms," *IEEE Trans. Signal Processing*, vol. 49, pp. 2774-2782, 2001.
- [27] Z.M. Hafed and M.D. Levine, "Face Recognition Using the Discrete Cosine Transform," *Int'l J. Computer Vision*, vol. 43, pp. 167-188, 2001.
- [28] C.M. Travieso, J.B. Alonso, and M.A. Ferrer, "Facial Identification Using Transformed Domain by SVM," *Proc. 38th Ann. Int'l Carnahan Conf. Security Technology*, pp. 321-324, 2004.
- [29] A.K. Fukunaga, *Introduction to Statistical Pattern Recognition*, second ed. Academic Press Professional, Inc., 1990.
- [30] W.K. Pratt, *Digital Image Processing*, second ed. John Wiley and Sons, 1991.
- [31] "CASIA Iris Image Database," <http://www.sinobiometrics.com>, 2007.
- [32] X. Liu, K.W. Bowyer, and P.J. Flynn, "Iris Recognition and Verification Experiments with Improved Segmentation Method," *Proc. Fourth IEEE Workshop Automatic Identification Advanced Technologies (AutoID)*, 2005.
- [33] H. Proença and L.A. Alexandre, "UBIRIS: Annoisy Iris Image Database," *Proc. Int'l Conf. Image Analysis and Processing*, vol. 1, pp. 970-977, 2005.
- [34] N.D. Kalka, J. Zuo, V. Dorairaj, N.A. Schmid, and B. Cukic, "Image Quality Assessment for Iris Biometric," *Proc. SPIE Conf. Biometric Technology for Human Identification III*, vol. 6202, pp. 61020D-1-62020D-11, 2006.
- [35] M. Dobes and L. Machala, "Iris Database," <http://www.inf.upol.cz/iris/>, 2007.
- [36] "MMU Iris Image Database: Multimedia Univ.," <http://pesona.mmu.edu.my/~ccteo/>, 2007.
- [37] "Univ. of Bath Iris Image Database," <http://www.bath.ac.uk/electeng/pages/sipg/irisweb/>, 2007.
- [38] "TLV's, Threshold Limit Values and Biological Exposure Indices for 1998," *Proc. Am. Conf. Governmental Industrial Hygienists*, 2001.
- [39] "Guidelines on Limits of Exposure for Broad-band Incoherent Optical Radiation (0.38 to 3  $\mu$ m), Health Phys," Int'l Commission on Nonionizing Radiation Protection (ICNIRP) 1997.
- [40] "British Standards Institute, Safety of Laser Products," BS EN 60825-1:1994, 1994.
- [41] P.K. Ryoung and K. Jaihie, "A Real-Time Focusing Algorithm for Iris Recognition Camera," *IEEE Trans. Systems, Man, and Cybernetics, Part C*, vol. 35, pp. 441-444, 2005.
- [42] N.F. Zhang, M.T. Postek, R.D. Larrabee, A.E. Vladar, W. Keery, and S.N. Jones, "A Statistical Measure of Image Sharpness for Scanning Electron Microscopes," *Scanning*, vol. 21, pp. 246-252, 1999.
- [43] H.J. Wyatt, "A 'Minimum-Wear-and-Tear' Meshwork for the Iris," *Vision Research*, vol. 40, pp. 2167-2176, 2000.
- [44] D.A. Newsome and I.E. Loewenfeld, "Iris Mechanics II: Influence of Pupil Size on Details of Iris Structure," *Am. J. Ophthalmology*, vol. 71, pp. 553-573, 1971.
- [45] A.J. Mansfield and J.L. Wayman, "Best Practices Standards for Testing and Reporting on Biometric Device Performance," technical report, Nat'l Physical Laboratory, Middlesex, U.K., 2002.



**Donald M. Monro** received the BSc (1964) and MSc (1966) degrees from the University of Toronto. He spent a brief period in the aeronautical industry before studying for the PhD degree at Imperial College, London, which was awarded in 1971, by which time he was a lecturer in electrical engineering. He is an emeritus professor in electronic and electrical engineering at the University of Bath, United Kingdom, and a consultant in signal processing

for biometrics. He was subsequently a senior lecturer in electrical engineering from 1979 and in the Department of Computing from 1983, both at Imperial College, before taking up the chair of electronics at the University of Bath in 1991. In addition to biometrics, his research interests are in digital video, and audio compression, and more general aspects of signal processing. He is a member of the IEEE.



**Soumyadip Rakshit** received the BTech degree in electronics and telecommunications engineering from Kalyani University, India, in 2004. Currently, he is a research student at the University of Bath, United Kingdom, specializing in iris recognition. His research interests include signal and image processing, statistical analysis, pattern recognition, biometrics, and matching pursuits. He is a student member of the IEEE.



**Dexin Zhang** received the BSc degree in automation engineering from Tsinghua University, and the MS degree from the National Laboratory of Pattern Recognition, Chinese Academy of Sciences, Beijing, China, in 2003. Currently, he is a research student at the University of Bath, United Kingdom, specializing in iris recognition. His research interests include biometrics, image processing, and pattern recognition. He is a student member of the IEEE.

▷ For more information on this or any other computing topic, please visit our Digital Library at [www.computer.org/publications/dlib](http://www.computer.org/publications/dlib).